CHINESE OPTICS LETTERS

Vol. 21, No. 8 | August 2023

Simultaneous wireless information and power transfer transmitting architecture based on asynchronous space-time-coding digital metasurface [Invited]

Zhen Jie Qi (祁振杰)[1,†], Jun Yan Dai (戴俊彦)[1,2,3,†*], Si Ran Wang (王思然)[1], Qun Yan Zhou (周群焰)[1], Wankai Tang (唐万恺)[4], Kaicen Wang (王凯岑)[1], Peng Zhang (张 澎)[5**], Shuo Liu (刘 硕)[1,2,3], Long Li (李 龙)[6], Qiang Cheng (程 强)[1,2,3***], and Tie Jun Cui (崔铁军)[1,2,3****]

[1] State Key Laboratory of Millimeter Waves, Southeast University, Nanjing 210096, China

[2] Institute of Electromagnetic Space, Southeast University, Nanjing 210096, China

[3] Frontiers Science Center for Mobile Information Communication and Security, Southeast University, Nanjing 210096, China

[4] National Mobile Communications Research Laboratory, Southeast University, Nanjing 210096, China

[5] National Key Laboratory of Electromagnetic Information Control and Effects, Shenyang 110035, China

[6] Key Laboratory of High-Speed Circuit Design and EMC of Ministry of Education, Xidian University, Xi'an 710071, China

*Corresponding author: junyand@seu.edu.cn

**Corresponding author: fanpure_yug@163.com

***Corresponding author: qiangcheng@seu.edu.cn

****Corresponding author: tjcui@seu.edu.cn

Received April 28, 2023 | Accepted June 26, 2023 | Posted Online August 7, 2023

Simultaneous wireless information and power transfer (SWIPT) architecture is commonly applied in wireless sensors or Internet of Things (IoT) devices, providing both wireless power sources and communication channels. However, the traditional SWIPT transmitter usually suffers from cross-talk distortion caused by the high peak-to-average power ratio of the input signal and the reduction of power amplifier efficiency. This paper proposes a SWIPT transmitting architecture based on an asynchronous space-time-coding digital metasurface (ASTCM). High-efficiency simultaneous transfer of information and power is achieved via energy distribution and information processing of the wireless monophonic signal reflected from the metasurface. We demonstrate the feasibility of the proposed method through theoretical derivations and experimental verification, which is therefore believed to have great potential in wireless communications and the IoT devices.

Keywords: simultaneous wireless information and power transfer; asynchronous space-time-coding digital metasurface; quadrature phase-shift keying modulation.

DOI: 10.3788/COL202321.080005

1. Introduction

With the development of the Internet of Things (IoT), more and more wireless terminals have been involved, causing an incredible increase in power consumption, even if they are so-called low-power devices. Wireless power transfer provides an effective solution for power transfer in the field of low-power and medium/long-distance transmission. On this basis, simultaneous wireless information and power transfer (SWIPT) is proposed to convey both information and energy by electromagnetic (EM) waves, enabling simultaneous communication and charging of low-power IoT devices[1–7]. However, the conventional SWIPT transmitter suffers from cross-talk distortion caused by the high peak-to-average power ratio[8] of the input signal and the reduced efficiency[9] of the power amplifier, which severely limits its performance[10].

Over the past two decades, metasurfaces have demonstrated unparalleled advantages in wireless communication, EM imaging, and so on[11–17]. With the introduction of coding metasurface comprising binary or multi-bit meta-atoms with finite phase states[18,19], amplitude and phase modulation can be dynamically realized easily with the aid of a field-programmable gate array (FPGA)[20–22]. Therefore, coding metasurfaces are widely applied to realize many functions, such as broadband diffusion, beam deflection, and holographic imaging[23–33]. Furthermore, recent advances in the time-domain-coding digital metasurface (TDCM) demonstrate tremendous potential for

harmonic generation with a high conversion efficiency, which paves the way for frequency modulation (FM) in the target spectrum[34–37].

Recently, the proposal of a space-time-coding digital metasurface (STCM) owning both temporal and spatial degrees of freedom has attracted extensive attention[36]. STCM demonstrates excellent flexibility in modulating harmonic amplitude, phase, and polarization simultaneously by assigning predesigned specific STC matrix on the metasurface[38–44]. However, the great majority of current STCM-based applications are performed under synchronous control. In other words, all meta-atoms change their states at the same frequency. In order to integrate more functions to fit for more application scenarios, the concept of asynchronous space-time-coding digital metasurface (ASTCM) is proposed with great advantages in automatic spatial scanning and dynamic scattering control[45]. Specifically, based on the unique property of function integration, the ASTCM will become a great candidate for SWIPT applications.

Based on ASTCM, we can easily adopt a spatial-division multiplexing strategy on the metasurface, that is, a significant portion of the metasurface is used for beamforming to achieve the purpose of power transfer, while the remaining meta-atoms are used for information modulation and transmission.

In this paper, we present a SWIPT architecture based on ASTCM, which offers the capability to transmit energy and information simultaneously. By designing the phase distribution in the space- and time-domain, respectively, a portion of the metasurface is used for beamforming to achieve directional power transfer, while another portion is responsible for harmonic manipulation to complete the information modulation. Since the power transfer and information transmission are orthogonal to each other in the frequency domain, no interference will be generated to affect the system performance. Finally, for experiment validation, a 3-bit metasurface is used to implement the SWIPT transmitter, considering its stability to the angle of the incident wave[46]. The results confirm the reliability of the proposed SWIPT transmitter based on ASTCM, which is believed to have great potential in the field of wireless communication as well as in IoT devices.

2. Theories and Simulations

As illustrated in Fig. 1, we assume that an ASTCM contains $M \times N$ meta-atoms, the state of which can be changed by altering the bias voltage of the embedded varactor diodes. Under the normal incidence of a monophonic wave at the frequency of f_c, the far-field scattering pattern of ASTCM can be written as[45]

$$f(t,R,\theta,\varphi)=\sum_{k=-\infty}^{\infty}\sum_{m=1}^{M}\sum_{n=1}^{N}E_{mn}(\theta,\varphi)a_{mn}^{k}e^{jk\phi_{mn}}, \tag{1}$$

where $E_{mn}(\theta,\varphi)$ represents the meta-atom's scattering pattern, and a_{mn}^{k} is the Fourier coefficient of the kth-order harmonic. θ and φ denote the elevation and azimuth angles, respectively. ϕ_{mn} stands for the time-invariant phase distribution, which can be expressed as

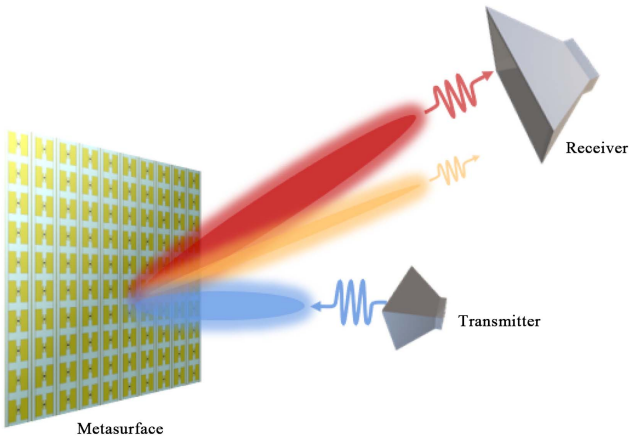

Fig. 1. Schematic of SWIPT based on the ASTCM under the excitation of a transmitter. The reflected waves form two beams for energy and information transmission, respectively, by tuning the phase states of the meta-atoms.

$$\phi_{mn}=\frac{2\pi f_c}{c}d((m-1)\sin\theta\cos\varphi+(n-1)\sin\theta\sin\varphi). \tag{2}$$

According to Eq. (1), the scattering patterns of harmonics can be synthesized through the design of the ASTC matrix, which is promising for efficiently realizing the directional power transfer.

Next, assume that every cycle of the time-varying reflection coefficient $\Gamma_{mn}(t)$ is uniformly divided into S time slots, each of which has a fixed reflection coefficient Γ_s, namely, the ASTC matrix; then the reflection coefficient in a cycle form can be written as

$$\Gamma_{mn}(t)=\sum_{s=0}^{S-1}\Gamma_s g(t-s\tau),\quad 0\le t\le T_{mn}, \tag{3}$$

where T_{mn} stands for cycles of each coding sequence, and $g(t)$ is a periodic unit pulse function of width $\tau=T_{mn}/S$ with a Fourier series expansion as

$$g(t)=\sum_{k=-\infty}^{\infty}\frac{1}{S}\mathrm{Sa}\left(\frac{k\pi}{S}\right)e^{-j\frac{k\pi}{S}}e^{jkf_0t}, \tag{4}$$

where $\mathrm{Sa}(\frac{k\pi}{S})=\sin(\frac{k\pi}{S})/\frac{k\pi}{S}$ is the sampling function. By substituting Eq. (4) back into Eq. (3), the Fourier series of the reflection coefficients can be obtained as

$$\Gamma(f)=\sum_{k=-\infty}^{\infty}\mathrm{PF}\cdot\mathrm{TF}\cdot e^{jk2\pi f_0t}, \tag{5}$$

where

$$\mathrm{PF}=\frac{1}{S}\mathrm{Sa}\left(\frac{k\pi}{S}\right)e^{-j\frac{k\pi}{S}},\quad \mathrm{TF}=\sum_{s=0}^{S-1}\Gamma_s e^{-jk\frac{2s\pi}{S}}. \tag{6}$$

The spectra of the reflection coefficient with different bit width are respectively shown in Fig. 2. Obviously, as the bit

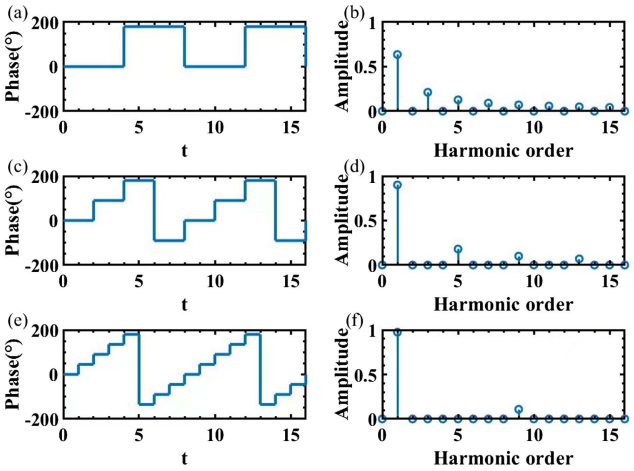

Fig. 2. Time-domain waveforms and amplitude spectra of the reflection coefficient with different bit width: (a), (b) 1-bit, (c), (d) 2-bit, and (e), (f) 3-bit.

width increases, the undesired harmonics will appear in higher order with lower energy and more energy will be converted to the +1st-order harmonic. Therefore, it is reasonable to infer that if we modulate the information at the +1st-order harmonic with a wide bit width, a high signal-to-noise ratio (SNR) and good signal quality can be guaranteed accordingly. In addition, the time-shift property of the Fourier transform can be further introduced to obtain phase modulation of the harmonics, which is expressed as follows[47]:

$$\Gamma(t - t_0) \leftrightarrow \Gamma(f)e^{-j2\pi t_0 f}. \tag{7}$$

Equation (7) indicates that a phase shift of $-2\pi t_0 f$ will be introduced in the frequency domain when the ASTC matrix loaded onto the metasurface produces a time shift of t_0. It enables us to efficiently perform phase-shift keying (PSK) modulation schemes at the +1st-order harmonic, thereby demonstrating the simultaneous transfer of information and power to verify the feasibility of the SWIPT transmitter.

3. Experiment Validations

In order to validate our method experimentally, we use the angle-insensitive 3-bit meta-atom in Ref. [46] for the construction of the SWIPT transmitter. The fabricated metasurface has 16 × 16 meta-atoms with the size of 404.6 mm × 435.2 mm. The structural parameters of each meta-atom are P_x = 25.4 mm, P_y = 27.2 mm, L_1 = 19.9 mm, L_2 = 8.8 mm, L_3 = 4.2 mm, W_1 = 0.4 mm, W_2 = 1.1 mm, and W_3 = 6.9 mm, as shown in Fig. 3. The reflection phase of the metasurface can be changed to cover the range of 0° to 315° at 3.15 GHz by controlling the voltage at both ends of the varactor diodes loaded on the meta-atoms. In this case, eight states of phase are chosen, namely, 0°, 45°, 90°, 135°, 180°, 225°, 270°, and 315°, to offer a 3-bit phase accuracy.

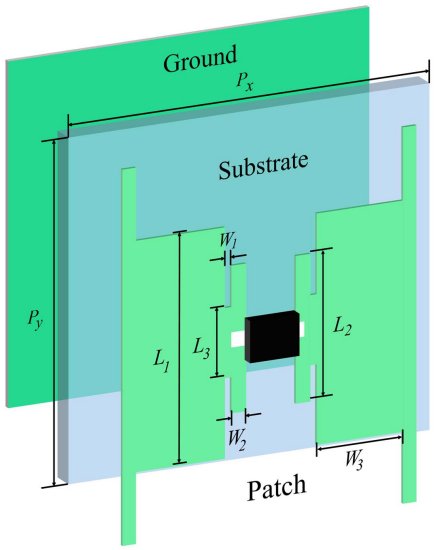

Fig. 3. Schematic of the 3-bit meta-atom, in which the substrate is sandwiched by two patches bridged by a varactor diode and a PEC ground. Different coding states can be obtained by changing the biasing voltage of the varactor diode.

Since the energy may need to be transmitted directionally to the IoT device, while the information is desired to be transmitted in all directions, the ASTC matrix is designed to apply a space-coding sequence to most of the meta-atom columns for directional power transfer, and time-coding sequence to the remaining columns for information transmission. Therefore, during the experiment, the ratio of meta-atom columns for two functions is designed to be 15:1, allocating the most resources for power transfer while maintaining the capability of wireless communication. According to Eq. (1), for a given azimuth angle in the power transfer, the scattering patterns of the fundamental frequency can be synthesized based on the phase distribution on the metasurface, which guides the generation of the control signal loaded on the varactor diode of each meta-atom by the FPGA. In addition, to guarantee a relatively good signal quality when transmitting information by 1-column meta-atoms, the +1st harmonic component carrying a relatively high energy is chosen here to modulate and transmit the information. Furthermore, the QPSK modulation scheme is implemented for demonstration, owing to its stable amplitude distribution during signal modulation. Based on the modulation regulation, the QPSK modulation scheme requires four different harmonic phases to represent four message symbols, each of which corresponds to a piece of 2-bit digital information. According to Eq. (7), the phase shifts generated by the +1st-order harmonic at different time shifts are listed in Table 1. It clearly shows the four different cyclic time shifts to be introduced into the loaded ASTC matrix, and the corresponding four message symbols stand for "00," "01," "10," and "11," respectively.

Figure 4 illustrates the schematic of directional power transfer and omnidirectional information transmission under the spatial-division multiplexing strategy, and four message symbols corresponding to the ASTC matrix with different cyclic

Table 1. Time Shift of Each Symbol and Phase Shift of the +1st-Order Harmonic.

Symbol	Cyclic Time Shift	Phase Shift at +1st order
00	0	0°
01	$T_{mn}/4$	−90°
10	$T_{mn}/2$	−180°
11	$3T_{mn}/4$	−270°

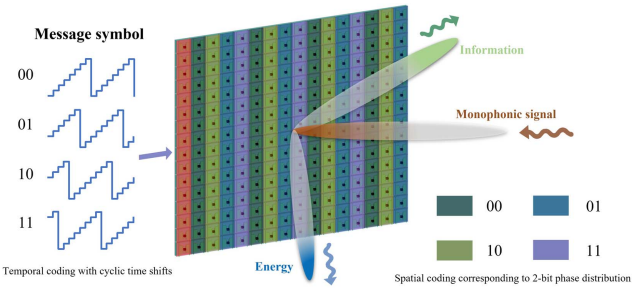

Fig. 4. Schematic of directional power transfer and omnidirectional information transmission under spatial-division multiplexing strategy.

time shifts. Since only space-coding sequences are applied on the meta-atoms for the power transfer, the energy is all transmitted at the fundamental frequency without any leakage to the harmonic, thus ensuring the maximum utilization of energy. Moreover, the +1st-order harmonic with a high power level also provides good signal quality for wireless communication, ensuring the realization of SWIPT.

To validate the performance of the proposed method, a SWIPT transmitter is constructed using the PXI (PCI extensions for instrumentation) system from National Instruments (NI). The carrier signal of a specific frequency, generated by a microwave signal generator (Agilent E8257D), is incident on the ASTCM through a feed horn. The control platform (NI PXIe-1082), which integrates an FPGA module (NI PXIe-7976), an I/O module (NI 5783), and a synchronized clock module (NI PXIe-6674 T), is programmed to generate the control signals corresponding to the ASTC matrix and then load them onto both ends of the varactor diodes on the metasurface through a customized amplification circuit. At the receiving terminal, a software-defined radio reconfigurable device (NI USRP-2943) is used as the receiver for data processing and analysis.

The QPSK modulation of the +1st-order harmonic is performed using the ASTC matrix at a modulation frequency f_0 of 500 kHz and an incident carrier frequency f_c of 3.15 GHz. The normalized spectrum distribution and the constellation diagram at the receiver terminal are shown in Fig. 5, respectively. Obviously, the amplitude of the fundamental frequency is 54 dB higher than that of the +1st-order harmonic. It is worth emphasizing that the amplitude ratio can be further customized by

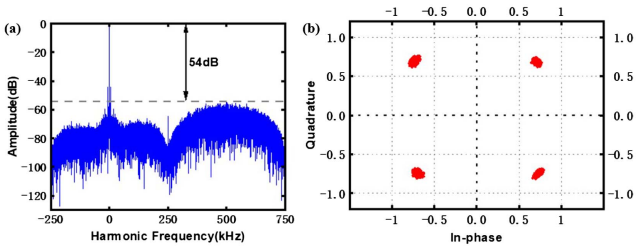

Fig. 5. (a) Spectral distribution of fundamental and +1st-order harmonic. (b) Constellation diagram measured at +1st-order harmonic for QPSK modulation scheme.

controlling the number of meta-atoms used, respectively, for power transfer and information transmission. In addition, as can be seen from Fig. 5(b), four sets of constellation points at the +1st-order harmonic are, respectively, located in the four quadrants of the constellation diagram, indicating a QPSK modulation scheme with slight deviations. This is due to the insufficient energy of the +1st-order harmonic that decreases the SNR of the wireless channel and leads to performance deterioration.

Finally, in order to make the power transfer more visible, we use an RF rectifier circuit loaded by a light-emitting diode (LED) array for demonstration, as shown in Fig. 6. The energy stream is generated by a monophonic EM wave from a signal generator, amplified by a power amplifier, transmitted through a horn antenna, and then incident normally to the ASTCM. With the modulation of the ASTC matrix, the EM wave of the carrier frequency f_c is beamformed and reflected towards 45°, where a receiving antenna captures and conveys the energy stream to the rectifier circuit, converting the RF energy to DC energy, and finally lighting up the LED array of "SEU." Meanwhile, we also use a video resource as the baseband data for information transmission validation. As shown in Fig. 6, the data stream is received fluently at the receiving terminal and then is presented in real time during the experiment. In the experiment, the video data transmission rate is 1 Mbit/s. In the meanwhile, we have 28 LEDs, and the DC power is 50.4 mW. Obviously, the experimental results fully show the good performance of our proof-of-concept prototype, demonstrating its enormous potential in SWIPT applications.

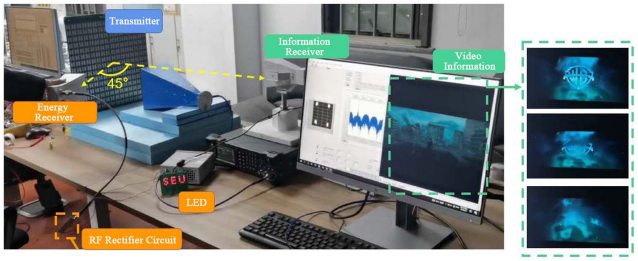

Fig. 6. Experimental demonstration of SWIPT based on the proposed architecture.

4. Conclusion

In this paper, we propose a spatial-division multiplexing SWIPT transmitter based on the ASTCM. Specifically, we design the ASTC matrix with spatial-division multiplexing strategies. The performance of the method is validated by a proof-of-concept prototype using a 3-bit metasurface. During the experiment, the constructed demonstration system can transmit information and energy simultaneously in different directions at different frequencies. In wireless communication, QPSK modulation is performed using the ASTC matrix to realize real-time video transmission. While in the power transfer, the ASTCM reflects high-power EM waves directionally to the receiving terminal, and the received energy is efficiently converted by the rectifier circuit to light up the LED array. The final experiments demonstrate the feasibility of this ASTCM-based SWIPT architecture, which effectively avoids cross-talk distortion caused by the high peak-to-average power ratio of the input signal and the reduced efficiency of the power amplifier. Although QPSK modulation is demonstrated in this architecture, more modulation methods can be introduced to make the architecture adaptable for more practical applications.

Acknowledgement

This work was supported by the Program of Song Shan Laboratory (included in the management of Major Science and Technology Program of Henan Province) (Nos. 221100211300-03 and 221100211300-02), the National Key Research and Development Program of China (No. 2018YFA0701904), the National Natural Science Foundation of China (Nos. 62288101, 61731010, 62201139, and U22A2001), the 111 Project (No. 111-2-05), the Jiangsu Province Frontier Leading Technology Basic Research Project (No. BK20212002), the Fundamental Research Funds for the Central Universities (No. 2242022k60003), the National Natural Science Foundation (NSFC) for Distinguished Young Scholars of China (No. 62225108), and the Southeast University - China Mobile Research Institute Joint Innovation Center (No. R207010101125D9).

†These authors contributed equally to this work.

References

1. J. Han, L. Li, X. Ma, X. Gao, Y. Mu, G. Liao, Z. J. Luo, and T. J. Cui, "Adaptively smart wireless power transfer using 2-bit programmable metasurface," IEEE Trans. Ind. Electron. **69**, 8524 (2022).
2. L. Li, H. Liu, H. Zhang, and W. Xue, "Efficient wireless power transfer system integrating with metasurface for biological applications," IEEE Trans. Ind. Electron. **65**, 3230 (2018).
3. S. C. Tian, X. M. Zhang, X. Wang, J. Q. Han, and L. Li, "Recent advances in metamaterials for simultaneous wireless information and power transmission," Nanophotonics **11**, 1697 (2022).
4. X. Wu, H. Xue, S. Zhao, J. Han, M. Chang, H. Liu, and L. Li, "Accurate and efficient method for analyzing the transfer efficiency of metasurface-based wireless power transfer system," IEEE Trans. Antennas Propag. **71**, 783 (2023).
5. H. Xue, X. Wu, X. Cui, M. Chang, H. Liu, L. Li, and T. J. Cui, "Multitarget wireless power transfer system using metasurface for quasi-bessel beams with large half power beam length," IEEE Trans. Microw. Theory Tech. **70**, 4449 (2022).
6. J.-H. Xun, Y. Mu, K. Zhang, H. Liu, and L. Li, "The efficiency improvement of multiple receivers in wireless power transmission by integrating metasurfaces," Materials **15**, 6943 (2022).
7. M. Chang, J. Han, X. Ma, H. Xue, X. Wu, L. Li, and T. Cui, "Programmable metasurface for simultaneously wireless information and power transfer system," ZTE Commun. **20**, 48 (2022).
8. B. Clerckx, R. Zhang, R. Schober, D. W. K. Ng, D. I. Kim, and H. V. Poor, "Fundamentals of wireless information and power transfer: from RF energy harvester models to signal and system designs," IEEE J. Sel. Areas Commun. **37**, 4 (2019).
9. Y. Rahmatallah and S. Mohan, "Peak-to-average power ratio reduction in OFDM systems: a survey and taxonomy," IEEE Commun. Surv. Tutor. **15**, 1567 (2013).
10. H. H. Jang, K. W. Choi, and D. I. Kim, "Novel frequency-splitting SWIPT for overcoming amplifier nonlinearity," IEEE Wirel. Commun. Lett. **9**, 826 (2020).
11. C. Wang, B. Li, S. Liu, Z. Zhang, and D. Zhao, "1-bit reconfigurable metasurface unit based on resonant coupling," in *IEEE 5th International Conference on Electronics Technology* (2022), p. 79.
12. Y. Saifullah, F. Zhang, G.-M. Yang, and F. Xu, "3-bit programmable reflective metasurface," in *12th International Symposium on Antennas, Propagation and EM Theory* (2018), p. 1.
13. J. Zhao, Q. Cheng, J. Chen, M. Q. Qi, W. X. Jiang, and T. J. Cui, "A tunable metamaterial absorber using varactor diodes," New J. Phys. **15**, 043049 (2013).
14. C. Dehos, J. L. González, A. De Domenico, D. Kténas, and L. Dussopt, "Millimeter-wave access and backhauling: the solution to the exponential data traffic increase in 5G mobile communications systems," IEEE Commun. Mag. **52**, 88 (2014).
15. W. Roh, J.-Y. Seol, J. Park, B. Lee, J. Lee, Y. Kim, J. Cho, K. Cheun, and F. Aryanfar, "Millimeter-wave beamforming as an enabling technology for 5G cellular communications: theoretical feasibility and prototype results," IEEE Commun. Mag. **52**, 106 (2014).
16. R. W. Heath, N. González-Prelcic, S. Rangan, W. Roh, and A. M. Sayeed, "An overview of signal processing techniques for millimeter wave MIMO systems," IEEE J. Sel. Top. Signal Process. **10**, 436 (2016).
17. X. Wan, M. Q. Qi, T. Y. Chen, and T. J. Cui, "Field-programmable beam reconfiguring based on digitally-controlled coding metasurface," Sci. Rep. **6**, 20663 (2016).
18. H. Yang, X. Cao, F. Yang, J. Gao, S. Xu, M. Li, X. Chen, Y. Zhao, Y. Zheng, and S. Li, "A programmable metasurface with dynamic polarization, scattering, and focusing control," Sci. Rep. **6**, 35692 (2016).
19. L. Li, H. Ruan, C. Liu, Y. Li, Y. Shuang, A. Alù, C.-W. Qiu, and T. J. Cui, "Machine-learning reprogrammable metasurface imager," Nat. Commun. **10**, 1082 (2019).
20. Y. B. Li, L. L. Li, B. B. Xu, W. Wu, R. Y. Wu, X. Wan, Q. Cheng, and T. J. Cui, "Transmission-type 2-bit programmable metasurface for single-sensor and single-frequency microwave imaging," Sci. Rep. **6**, 23731 (2016).
21. T. J. Cui, M. Q. Qi, X. Wan, J. Zhao, and Q. Cheng, "Coding metamaterials, digital metamaterials and programmable metamaterials," Light Sci. Appl. **3**, e218 (2014).
22. C. Della Giovampaola and N. Engheta, "Digital metamaterials," Nat. Mater. **13**, 1115 (2014).
23. T. Debogovic and J. Perruisseau-Carrier, "Low loss MEMS-reconfigurable 1-bit reflectarray cell with dual-linear polarization," IEEE Trans. Antennas Propag. **62**, 5055 (2014).
24. C. Huang, B. Sun, W. Pan, J. Cui, X. Wu, and X. Luo, "Dynamical beam manipulation based on 2-bit digitally-controlled coding metasurface," Sci. Rep. **7**, 42302 (2017).
25. L.-H. Gao, Q. Cheng, J. Yang, S.-J. Ma, J. Zhao, S. Liu, H.-B. Chen, Q. He, W.-X. Jiang, H.-F. Ma, Q.-Y. Wen, L.-J. Liang, B.-B. Jin, W.-W. Liu, L. Zhou, J.-Q. Yao, P.-H. Wu, and T.-J. Cui, "Broadband diffusion of terahertz waves by multi-bit coding metasurfaces," Light Sci. Appl. **4**, e324 (2015).
26. J. Zhao, X. Yang, J. Y. Dai, Q. Cheng, X. Li, N. H. Qi, J. C. Ke, G. D. Bai, S. Liu, S. Jin, A. Alù, and T. J. Cui, "Programmable time-domain digital-coding

metasurface for non-linear harmonic manipulation and new wireless communication systems," Natl. Sci. Rev. **6**, 231 (2019).
27. L. Li, T. Cui, W. Ji, S. Liu, J. Ding, X. Wan, Y. B. Li, M. Jiang, C.-W. Qiu, and S. Zhang, "Electromagnetic reprogrammable coding-metasurface holograms," Nat. Commun. **8**, 197 (2017).
28. Y. Yang, W. Wang, P. Moitra, I. I. Kravchenko, D. P. Briggs, and J. Valentine, "Dielectric meta-reflectarray for broadband linear polarization conversion and optical vortex generation," Nano Lett. **14**, 1394 (2014).
29. M. Liu, D. A. Powell, Y. Zarate, and I. V. Shadrivov, "Huygens' metadevices for parametric waves," Phys. Rev. X **8**, 031077 (2023).
30. A. Shaltout, A. Kildishev, and V. Shalaev, "Time-varying metasurfaces and Lorentz non-reciprocity," Opt. Mater. Express **5**, 2459 (2015).
31. J. Li, P. Yu, S. Zhang, and N. Liu, "Electrically-controlled digital metasurface device for light projection displays," Nat. Commun. **11**, 7 (2020).
32. J. Liao, S. Guo, L. Yuan, C. Ji, C. Huang, and X. Luo, "Independent manipulation of reflection amplitude and phase by a single-layer reconfigurable metasurface," Adv. Opt. Mater. **10**, 2101551 (2022).
33. L. Yuan, C. Huang, J. Liao, C. Ji, J. Huang, Y. Wang, and X. Luo, "A dynamic thermal camouflage metadevice with microwave scattering reduction," Adv. Sci. **9**, 2201054 (2022).
34. Z. Miao, Q. Wu, X. Li, Q. He, K. Ding, Z. An, Y. Zhang, and L. Zhou, "Widely tunable terahertz phase modulation with gate-controlled graphene metasurfaces," Phys. Rev. X **5**, 041027 (2015).
35. J. Y. Dai, J. Zhao, Q. Cheng, and T. J. Cui, "Independent control of harmonic amplitudes and phases via a time-domain digital coding metasurface," Light Sci. Appl. **7**, 90 (2018).
36. L. Zhang, X. Q. Chen, S. Liu, Q. Zhang, J. Zhao, J. Y. Dai, G. D. Bai, X. Wan, Q. Cheng, G. Castaldi, V. Galdi, and T. J. Cui, "Space-time-coding digital metasurfaces," Nat. Commun. **9**, 4334 (2018).
37. J. Y. Dai, W. K. Tang, J. Zhao, X. Li, Q. Cheng, J. C. Ke, M. Z. Chen, S. Jin, and T. J. Cui, "Metasurfaces: Wireless communications through a simplified architecture based on time-domain digital coding metasurface," Adv. Mater. Technol. **4**, 1970037 (2019).
38. L. Zhang, X. Q. Chen, R. W. Shao, J. Y. Dai, Q. Cheng, G. Castaldi, V. Galdi, and T. J. Cui, "Breaking reciprocity with space-time-coding digital metasurfaces," Adv. Mater. **31**, 1904069 (2019).
39. J. Y. Dai, W. Tang, M. Z. Chen, C. H. Chan, Q. Cheng, S. Jin, and T. J. Cui, "Wireless communication based on information metasurfaces," IEEE Trans. Microw. Theory Tech. **69**, 1493 (2021).
40. J. Y. Dai, J. Yang, W. Tang, M. Z. Chen, J. C. Ke, Q. Cheng, S. Jin, and T. J. Cui, "Arbitrary manipulations of dual harmonics and their wave behaviors based on space-time-coding digital metasurface," Appl. Phys. Rev. **7**, 041408 (2020).
41. J. Y. Dai, L. X. Yang, J. C. Ke, M. Z. Chen, W. Tang, X. Li, M. Chen, Z. H. Wu, Q. Cheng, S. Jin, and T. J. Cui, "High-efficiency synthesizer for spatial waves based on space-time-coding digital metasurface," Laser Photonics Rev. **14**, 1900133 (2020).
42. J. C. Ke, J. Y. Dai, M. Z. Chen, L. Wang, C. Zhang, W. Tang, J. Yang, W. Liu, X. Li, Y. Lu, Q. Cheng, S. Jin, and T. J. Cui, "Linear and nonlinear polarization syntheses and their programmable controls based on anisotropic time-domain digital coding metasurface," Small Struct. **2**, 2000060 (2021).
43. J. Y. Dai, W. Tang, M. Wang, M. Chen, Q. Cheng, S. Jin, T. J. Cui, and C. H. Chan, "Simultaneous *in situ* direction finding and field manipulation based on space-time-coding digital metasurface," IEEE Trans. Antennas Propag. **70**, 4774 (2022).
44. X. Wan, J. W. Wang, Z. A. Huang, B. Y. Li, Q. Xiao, and T. J. Cui, "Space-time-frequency modulation mechanisms of monochromatic and nonmonochromatic electromagnetic waves on a digital programmable transmission metasurface," Adv. Funct. Mater. **32**, 2107557 (2022).
45. S. R. Wang, M. Z. Chen, J. C. Ke, Q. Cheng, and T. J. Cui, "Asynchronous space-time-coding digital metasurface," Adv. Sci. **9**, 2200106 (2022).
46. J. C. Liang, Q. Cheng, Y. Gao, C. Xiao, S. Gao, L. Zhang, S. Jin, and T. J. Cui, "An angle-insensitive 3-bit reconfigurable intelligent surface," IEEE Trans. Antennas Propag. **70**, 8798 (2022).
47. J. Y. Dai, W. Tang, L. X. Yang, X. Li, M. Z. Chen, J. C. Ke, Q. Cheng, S. Jin, and T. J. Cui, "Realization of multi-modulation schemes for wireless communication by time-domain digital coding metasurface," IEEE Trans. Antennas Propag. **68**, 1618 (2020).